

## 1. Data Sources

Our study is based on seismic data from a collection of observatories operated in eastern North America for periods of time from over a decade to 18-24 months. All data used are archived at the IRIS Data Management Center ([ds.iris.edu](https://ds.iris.edu)). Information on individual networks is provided in table DR1.

Network Name	Web address
Earthscope Transportable Array	<a href="https://doi.org/10.7914/SN/TA">doi:10.7914/SN/TA</a>
Lamont-Doherty Cooperative Seismographic Network	<a href="http://ds.iris.edu/mda/LD">http://ds.iris.edu/mda/LD</a>
New England Seismic Network	<a href="https://doi.org/10.7914/SN/NE">doi:10.7914/SN/NE</a>
US National Seismic Network	<a href="https://doi.org/10.7914/SN/US">doi:10.7914/SN/US</a>

**Table DR1.** Seismic Networks used in this study. Last two letters of the web and/or DOI address designate the network, and are also shown in table T1 of the main text.

## 2. Methods for evaluating shear wave splitting.

An expected effect of shear wave propagation through the anisotropic medium is the partition (known as splitting) of the shear wave into fast and slow components aligned with, and normal to, the symmetry axis of the anisotropic velocity (Crampin, 1977). Using shear waves that passed through the Earth's liquid outer core (labeled SKS, SKKS, SKIKS and PKS, called XKS collectively, Storchak et al., 2003), and are therefore polarized in the vertical plane when they enter the upper mantle, allows for a straightforward analysis strategy based on detection and quantification of the horizontally polarized energy within the same waveform (Savage, 1999). This energy is treated as reflective of splitting due to anisotropy.

We employ three different algorithms to evaluate the effect of shear wave speed anisotropy on the particle motion of the teleseismic shear wave. All three algorithms assume that the wave passes through a single volume with hexagonal anisotropy, where the symmetry axis is horizontal. Furthermore, we assume the symmetry axis to be the fastest direction, in accordance with expectations for the deformation-induced systematic orientation of olivine crystals in the upper mantle (Christensen, 1984; Ribe, 1992).

Two methods seek to determine the polarization of the fast component of the shear wave, and the delay of the slow component relative to it. The third method quantifies the energy of the horizontally polarized (Transverse) component of the XKS phase motion. Brief summaries of the methods are presented below. Detailed treatment of their performance is discussed by Long and Van der Hilst (2005), while their implementation in our processing algorithms are given by Wüstefeld and Bokelman (2007) and Deng et al., (2017).

2.1 Rotation-correlation method (RC). This technique assumes that an originally rectilinear particle motion of a shear wave is split into two orthogonal components, fast and slow, which have the same pulse shape, but travel with different speed. To identify the polarization of these components, two horizontal components of the recorded shear wave are rotated to a succession of trial orientations, and their pulse shapes are compared by means of cross-correlation. The rotation yielding the largest cross-correlation coefficient is taken to be the fast polarization, and the time where largest positive cross-correlation occurs is taken to be the delay.

2.2 Minimum transverse energy (SC). Named in honor of the publication Silver and Chan (1991), this method assumes that the original polarization of the XKS phase should be in the vertical plane containing the source and the receiver (component of motion labeled Q in figure DR1), and the energy on the horizontal component orthogonal to this plane (component labeled T in figure DR1) should be minimal. Two horizontal components of the recorded shear wave are rotated to a set of trial orientations, and shifted by a set of trial delays. Following each rotation and shift, timeseries are rotated back to Q and T orientations, and the total energy on the T component is evaluated. The combination of rotation and shift that yields the smallest T component is taken to represent the splitting parameters (fast polarization and delay).

2.3 Splitting Intensity (SI). This method also assumes original SV polarization in the recorded wave, and takes advantage of the fact that the T component of the motion in a split shear wave should resemble a time derivative of the Q component, with amplitude

proportional to both the wave propagation direction relative to the anisotropic symmetry axis, and the delay introduced by propagation through the anisotropic region.

Consequently, the strength (intensity) of splitting in an observed wave is quantified by the comparison of the recorded T component and the time derivative of the Q. SI values are then represented as a function of the backazimuth (direction from the receiver towards the source), and compared with expected patterns of functions in the form of  $a * \sin(2(x - b))$ .

Figure DR1 illustrates results of two measurements that include all three methods. For RC and SC methods error surfaces are presented showing the range of best-fitting solutions by shading. Results of SI measurements are presented as values, with error bars.

### **3. NULL splitting**

Figure DR1 presents measurements from the same phase obtained at two sites, one within the NAA (HNH) and another near its outer edge (UCCT). The pulse shape of an SKS phase is exceptionally simple, and provides a good example of the differences in observed data that yield observations of splitting (at UCCT) and NULL (at HNH). The amount of energy on the transverse component is visually smaller for HNH, and the particle motion diagram is nearly linear. The error surfaces for both RC and SC methods have characteristic shaded regions that extend through the entire range of delays tested, indicating no preference for a particular delay. On the other hand, at site UCCT there is a clear pulse on the T component, and the error surfaces show well-defined regions where the correlation is highest for RC method, and transverse energy is lowest for SC method. The SI values at these two sites differ by a factor of 10.

### **4. Results of all shear wave splitting measurements.**

Figure S3 shows all measurements we have performed in the form of stereo-maps for both RC and SC methods, emphasizing the differences in outcomes for sites where splitting is weak and incoherent (e.g. HNH) and similarity for those where it is stronger (e.g. NCB).

Table DR2 presents values and error ranges for all 622 observations we have produced.

### **5. Discrepancy between splitting values in SKS and SKKS phases from the same event.**

In a number of instances we find that two core-refracted phases (SKS and SKKS) from the same event observed at the same station yield significantly different outcomes in terms of shear wave splitting. In most, but not all, of them (table DR3) the SKS phase yields a NULL observation while the SKKS phase is split. The most plausible explanation for this discrepancy is the presence of significant azimuthal anisotropy in the D'' region of the lower mantle where the split phase comes out the core, and its absence in the region where the phase with a NULL measurement comes out.

#### References.

Christensen, N. I., The magnitude, symmetry and origin of upper mantle anisotropy based on fabric analyses of ultra- mafic tectonites, *Geophys. J. R. Astron. Soc.*, *76*, 89 –111, 1984.

Crampin, S., A review of the effects of anisotropy layering on the propagation of seismic waves, *Geophys. J. R. Astron. Soc.*, *45*, 9–27, 1977.

Deng, J., M. D. Long, N. Creasy, L. Wagner, S. Beck, G. Zandt, H. Tavera, and E. Minaya (2017), Lowermost mantle anisotropy near the eastern edge of the Pacific LLSVP: constraints from SKS-SKKS splitting intensity measurements, *Geophys. J. Int.*, *210*, 774-786, doi:10.1093/gji/ggx190.

Long, M. D., and R. D. van der Hilst, (2005) Estimating shear-wave plitting parameters from broadband recordings in Japan: a comparison of three methods , *Bulletin of the Seismological Society of America*, Vol. 95, No. 4, pp. 1346–1358

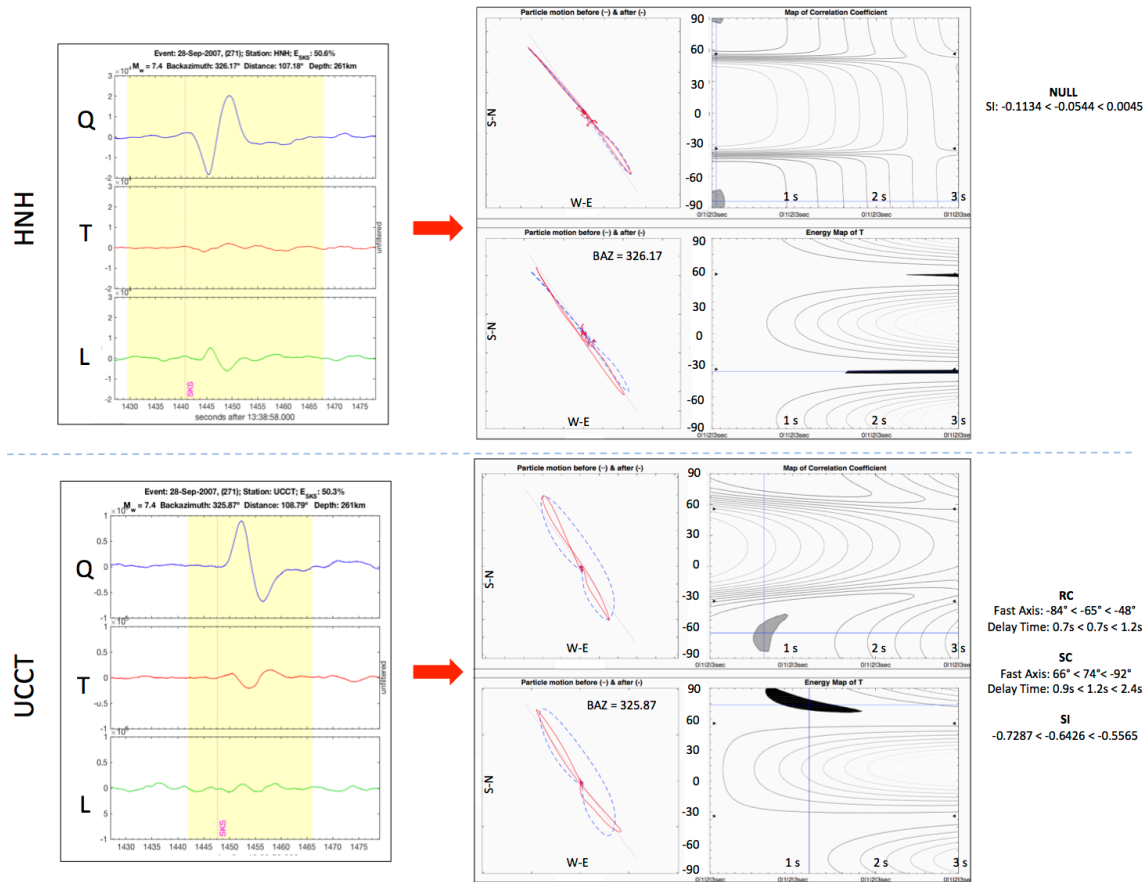
Ribe, N. M., On the relation between seismic anisotropy and finite strain, *J. Geophys. Res.*, *97*, 8737–8747, 1992.

Savage, M. K. Seismic anisotropy and mantle deformation: What have we learned from shear wave splitting? (invited contribution) *Reviews of Geophysics*, *37*, 65-106, 1999.

Storchak, D. A., Schweitzer, J., & Bormann, P. (2003). The IASPEI standard seismic phase list. *Seismological Research Letters*, 74(6), 761-772.

Wüstefeld, A., Bokelmann, G.H.R., 2007. Null detection in shear-wave splitting measurements. *Bull. Seism. Soc. Am.* 97 (4), 1204–1211, doi:10.1785/0120060190.

Figures.



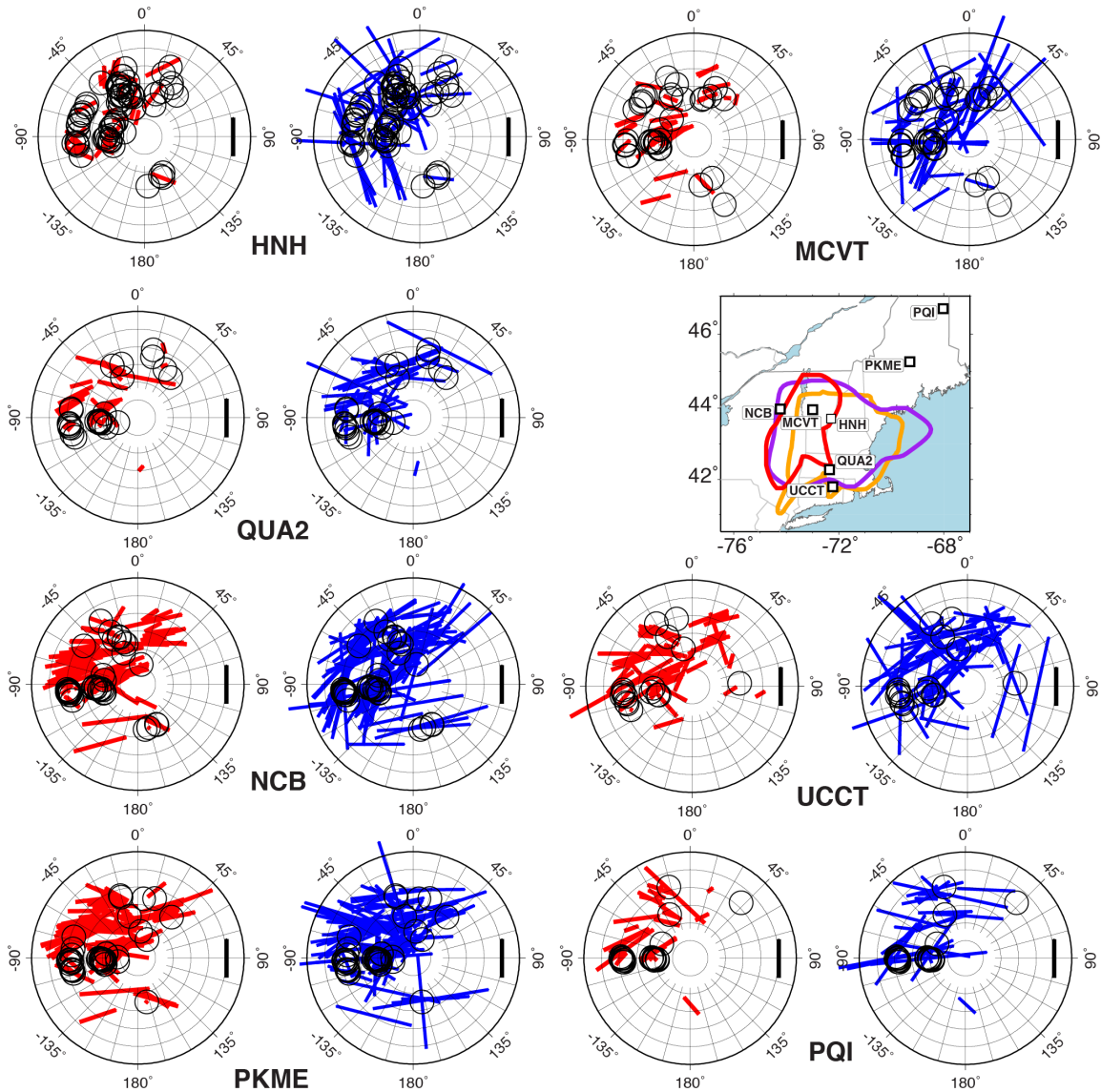


Figure DR2. All observations of shear wave splitting for seven long operating sites are presented in the form of stereo-maps. Each measurement is plotted at the position corresponding to its backazimuth and incidence angle. Grid lines in diagrams are  $15^\circ$  apart for backazimuth, and  $3^\circ$  for incidence angle. Splitting measurements are shown as bars aligned with the fast polarization (North is up, East is to the right), and scaled with delay (black bar at  $90^\circ$ ,  $15^\circ$  is 1 s long). NULL values are shown as circles. Observations from RC method are shown in red, those from SC method – in blue. An inset map shows locations of the sites and outlines of the North Appalachian Anomaly adopted from Schmandt and Lin (2014), Porter et al., (2016), and Menke et al.,(2016).

Table DR2

Table DR3

Station	Event Date	Depth (km)	Mw	BAZ	Distance	Phase I	Split?	Inclination	Fast Axis	Delay Time	Phase II	Split?	Inclination	Fast Axis	Delay Time	Quality
HNH	2007.271	261	7.4	326.17	107.18	SKS	N	7.49	-	-	SKKS	Y	12.15	-1.83	0.55	good
HNH	2007.197	351	6.8	338.37	96.16	SKS	N	9.06	-	-	SKKS	Y	12.65	13.37	0.5	fair/good
HNH	2009.264	14	6.01	15.17	107.75	SKS	N	7.47	-	-	SKKS	Y	12.16	63.17	1	fair/good
HNH	2009.313	591	7.3	270.3	115.64	SKS	N	6.42	-	-	SKKS	Y	11.65	50.3	0.7	good
HNH	2010.204	607	7.3	340.11	127.84	SKiKS	Y	3.53	12.96	0.35	SKKS	N	10.92	-	-	fair
HNH	2011.093	552	6.4	267.86	113.67	SKS	N	6.63	-	-	SKKS	Y	11.73	-48.14	0.65	fair
HNH	2012.024	583	6.4	263.36	120.29	SKS	N	5.88	-	-	SKKS	Y	11.42	-60.64	0.5	fair
MCVT	2014.215	13	6.8	310.88	123.37	SKS	Y	5.65	79.88	0.95	SKKS	N	11.31	-	-	fair/good
MCVT	2015.127	10	7	297	124.75	SKiKS	Y	3.52	77	0.65	SKKS	N	11.19	-	-	fair/good
QUA2	2013.131	205	6.4	264.66	111.15	SKS	N	7	-	-	SKKS	Y	11.98	45.66	0.3	fair/good
QUA2	2014.064	637	6.3	277.67	120.3	SKS	Y	5.86	53.67	0.4	SKKS	N	11.41	-	-	fair/good
QUA2	2016.104	135	6.9	12.83	113.86	SKS	Y	6.69	-79.17	1.45	SKKS	N	11.81	-	-	fair/good